Journal of Polymer Research (2019) 26: 275
https://doi.org/10.1007/s10965-019-1915-1

ORIGINAL PAPER

Effect of aspect ratio of multi-wall carbon nanotubes on the dispersion in ethylene-α-octene block copolymer and the properties of the Nanocomposites

Jing Qian[1] · Jun-Hong Pu[1] · Xiang-Jun Zha[1] · Rui-Ying Bao[1] · Zheng-Ying Liu[1] · Ming-Bo Yang[1] · Wei Yang[1]

Received: 17 March 2019 / Accepted: 15 September 2019 / Published online: 20 November 2019

Abstract

Effects of aspect ratio of multi-wall carbon nanotubes (MWCNTs) on the dispersion of MWCNTs in ethylene-α-octene block copolymer (OBC) and the properties of OBC/MWCNTs nanocomposites were studied, and two series of MWCNTs with different aspect ratios based on the same length and the same diameter were considered. Scanning electron microscope (SEM) and transmission electron microscope (TEM) results show that small and large agglomerates induced by intra- and inter-entanglement of MWCNTs are present for MWCNTs with high aspect ratio having smaller diameter and larger length, respectively. Rheological, electrical and tensile properties of OBC/MWCNTs nanocomposites are related to the aspect ratio and dispersion of MWCNTs. The formation of agglomerates, especially large agglomerates, influence the network perfection, weakening the contribution of MWCNTs to the rheology and electrical properties. The inter-entanglement shows less negative effect on the enhancement for the modulus and strength of OBC nanocomposites, and intra-entanglement of MWCNTs shows discounted enhancing properties. The aspect ratios of MWCNTs related to not only the length but also the diameter play the dominant role on the dispersion in polymers and the properties of polymer nanocomposites.

Keywords Multi-walled carbon nanotubes · Aspect ratio · Dispersion · Properties

Introduction

Since defined by Iijima in 1991 [1], carbon nanotubes (CNTs) which have a unique tubular structure with nanometer scale diameters and large length/diameter ratios, have attracted great interest in academia and industry for their practical applications. Structurally, a carbon nanotube can be considered as a cylinder of nanoscale diameter curled up at a certain angle by one or more layers of graphite. The sp^2 C-C bonds in carbon nanotubes give them perfect mechanical performance, and it is generally considered that the mechanical performance of CNTs has surpassed other materials we have known [2–4]. Theoretical and experimental results have demonstrated that the Young's modulus of CNTs is up to 1.2 TPa and the tensile modulus is 50–200 GPa. Apart from the mechanical properties, electrical and thermal properties of CNTs are also outstanding. Multi-walled carbon nanotubes (MWCNTs) have electrical conductivity about 10^3–10^5 s/m, and the theoretical thermal conductivity of MWCNTs is about 3000 Wm^{-1} k^{-1} [5, 6]. Researchers have tried to introduce MWCNTs into polymers to obtain polymer/MWCNTs nanocomposites by various strategies, and found that the mechanical and electrical performance of the composites can be greatly improved, compared to pristine polymers [7–15]. In this way, the polymer/MWCNTs nanocomposites are designed and developed for various applications such as conductive plastics, energy storage, thermally conductive materials, and so on [16–23].

The dispersion of MWCNTs in the polymer matrix greatly affects the performance of polymer/MWCNTs nanocomposites. Studies have shown that factors such as the

Electronic supplementary material The online version of this article (https://doi.org/10.1007/s10965-019-1915-1) contains supplementary material, which is available to authorized users.

✉ Rui-Ying Bao
rybao@scu.edu.cn

✉ Wei Yang
weiyang@scu.edu.cn

[1] College of Polymer Science and Engineering, State Key Laboratory of Polymer Materials Engineering, Sichuan University, Chengdu 610065, Sichuan, China

characteristics of the nanotubes and the nature of the polymers, the nanotube-nanotube and the nanotube–polymer interactions, and processing conditions, affect the dispersion and the formation of networks of MWCNTs in the nanocomposites. Nanotube structural characteristics, including aspect ratio, branching and curviness, and primary agglomerate morphology, affect the composites properties in terms of nanotube dispersion behavior and network formation ability. Krause [24] found branched carbon nanostructure (CNS) flakes can show excellent dispersability in polypropylene (PP), poly(vinylidene fluoride) (PVDF) and polycarbonate (PC) and branched-MWCNTs/polymer composites always exhibited lower percolation threshold than linear-MWCNTs/polymer composites due to the existence of junctions at branching points. For linear-MWCNTs, aspect ratio considering the influence of length or diameter usually was studied. Wu et al. [25] investigated the relations between the aspect ratio of MWCNTs with different lengths and the formation of percolation networks in polylactide (PLA)/MWCNTs composites. It was found that, at low loading levels, MWCNTs with low aspect ratio are dispersed as bent fibers or small bundles, whereas MWCNTs with high aspect ratio are dispersed as self-entangled flocs. At high loading levels, both are dispersed as flocs. MWCNTs with high aspect ratio impart more contributions to rheological and mechanical properties of PLA composites. Ayatollahi et al. [26] investigated the effects of the aspect ratio of MWCNTs with different diameters on the properties of epoxy/MWCNT nanocomposites. It was found that epoxy nanocomposites containing MWCNTs with smaller diameter presented better electrical and mechanical properties. MWCNTs with smaller diameter showed some agglomerates, while MWCNTs with bigger diameter exhibited a more homogeneous distribution.

The large length of MWCNTs and nanotube-nanotube interaction make the produced MWCNTs agglomerates, and the primary agglomerate morphology influences MWCNTs dispersion and distribution in the polymer and the performances of the nanocomposites. Krause et al. [27] studied the sedimentation of MWCNTs dispersed in aqueous surfactant solution at different ultrasonication treatment times to assess the dispersability of MWCNTs. It was founded that Nanocyl™ NC7000 and Baytubes® C150P were dispersed as single nanotubes after ultrasonic treatment, while small agglomerates or bundles existed in dispersions containing FutureCarbon CNT-MW and Graphistrength® C100. Krause et al. [28] also dispersed CNTs produced under different synthesis conditions in aqueous surfactant solutions and investigated the sedimentation behavior under centrifugation forces. The electrical percolation threshold of polyamide 66/CNTs composites was determined and the dispersion state of CNTs was studied after CNTs were melt mixed in polyamide 66. It was found that CNTs dispersed stably in aqueous surfactant solutions showed lower percolation threshold and better dispersion in polyamide 66.

It also should be noted that, the MWCNTs can be shortened during the processing [29–32]. Guo et al. [29] investigated the effects of MWCNTs aspect ratio on the electrical, and mechanical properties of the PC/MWCNTs composites melt mixed in a twin-screw conical micro compounder. It was found that, at such high aspect ratio 313 and 474, the electrical percolation thresholds of the composites were independent of the aspect ratio prior to melt mixing, due to the nanotubes were broken to the same average length. Menzer et al. [32] studied the influence of ball milling on the structural characteristics of MWCNTs and compared the dispersion and percolation threshold of MWCNTs before and after treated by ball milling in melt mixed nanocomposites using a maleic anhydride modified isotactic polypropylene as matrix. Ball milling made as-synthesised nanotubes be reduced in the length by half and their primary agglomerates be compacted significantly. It was suggested that electrical and rheological percolation thresholds of the composites containing the as-synthesised MWCNTs with longer length were lower than those treated by ball milling.

As viewed from application in the engineering fields, the effect of aspect ratio on the properties of the nanocomposites are not studied thoroughly and some confuses are still unsolved. Do the MWCNTs with high aspect ratios always impart more contributions to properties of the nanocomposites despite the agglomerates of MWCNTs? How the aspect ratios influence the properties of the nanocomposites when MWCNTs with different lengths and diameters are used simultaneously?

In our previous work, MWCNTs can achieve homogeneous dispersion in the form of single MWCNT in ethylene-α-octene block copolymer (OBC) by melting processing, possibly due to the different affinities of MWCNTs towards the soft and hard blocks of OBC [33, 34]. The phenomenon of homogeneous distribution of MWCNTs can also be observed in other polymer by melting processing [35, 36]. In this work, the effect of aspect ratio on the dispersion of MWCNTs in OBC and the rheological, electrical and tensile performances of OBC nanocomposites were studied, and two series of MWCNTs with different aspect ratios based on the same length and the same diameter were considered. The results show that the dispersion of MWCNTs is greatly influenced by the nanotube-nanotube and the nanotube-polymer interactions depending on the aspect ratios of MWCNTs related to not only the length but also the diameter of MWCNTs. The rheological, electrical, and tensile properties of the nanocomposites depend on not only the aspect ratios of MWCNTs, but also the dispersion state. This work is hopeful to provide guidance for the preparation of conductive and enhanced thermoplastic elastomers.

Experimental section

Materials

OBC (Infuse 9807), with a density of 0.866 g/cm^3 and melt flow rate of 15 g/10 min, was purchased from Dow Chemical Co. (Midland, MI, USA). MWCNTs (XFM01, XFM13, XFM16, XFM25) were purchased from XFNANO Inc. (Nanjing, China), and MWCNTs (TNIM-3) were purchased from Chengdu Institute of Organic Chemistry, Chinese Academy of Sciences (Chengdu, China). The density of MWCNTs is 2.1 g/cm^3. The information of MWCNTs stemming from the providers are listed in Table 1, and the aspect ratio was calculated from the mean values of the length and diameter. The primary morphology of MWCNTs were shown in Fig. S1. MWCNTs were used without further treatment, and the surface chemistry of all MWCNTs is similar.

Sample preparation

OBC and MWCNTs were melt compounded in an internal mixer (XSS-300, Shanghai Kechuang Rubber Plastics Machinery Set Ltd., China) with a rotor speed of 50 rpm at 150 °C for 8 min. After compounding, OBC nanocomposites were compression molded into sheets at 150 °C for 10 min under the pressure of 10 MPa. All the preparation processes were the same except for the type and content of MWCNTs, as the process could influence the morphology and distribution of MWCNTs. [37] The prepared nanocomposites were marked as SL-x-y or SD-x-y based on the characteristic of MWCNTs, where SL means the same length and SD means the same diameter, x represents the aspect ratio and y represents the content of MWCNTs.

Characterization

Dispersion of MWCNTs

The dispersion of MWCNTs in OBC was characterized with a JEOL JSM-5900LV scanning electron microscope (SEM, Japan) at an accelerating voltage of 20 kV and a transmission electron microscope (TEM, Philips CM120) equipped with a field emission gun (FEG) operating at 200 kV. For SEM characterization, the compression molded samples were cryo-fractured in liquid nitrogen, and the cross-section were coated with gold before the observation. For TEM characterization, ultrathin sample sections with a thickness of 50–100 nm were cut by a Leica EM UC6 ultramicrotome (Leica Microsystems, Wetzlar, Germany) at −120 °C form the cross-section of compression molded plates before observation.

Rheological measurements

Rheological measurements were carried out on a stress-controlled rotational rheometer (AR2000EX, TA Instruments, USA) in a dynamic frequency sweep from 0.01 to 100 Hz at a strain of 1% within the linear viscoelastic region at 150 °C. The compression molded plates with the thickness of 1.5 mm and the diameter of 25 mm were used for test.

Electrical conductivity

Electrical volume resistivity measurements were performed using a 2400 SourceMeter® (Keithley Instruments, Inc., Ohio, USA) combined with a test lead kit Model 1754 (Keithley Instruments, Inc., Ohio, USA) for resistivity values lower than 10^6 Ohm. A high-resistivity meter (ZC36, Shanghai Precision Instruments Co., Ltd. China) was used for values higher than 10^6 Ohm. The compression molded rectangular sheets with the dimensions of 30 mm × 10 mm × 2 mm (both sides of the samples were coated with silver paste to reduce the contact resistance) were measured by the digital multi-meter and the circle wafers with the diameter of 150 mm and the thickness of 1.2 mm were measured by the high-resistivity meter. At least five samples were tested for each measurement and the average results were reported.

Tensile tests

Tensile tests were conducted on a universal tensile instrument (Model 5967, Instron Instrument, USA) at a cross-head speed of 100 mm/min at room temperature with a gauge length of 10 mm. The dumb-bell samples with the

Table 1 Information of the used MWCNTs

	Same length (SL)			Same diameter (SD)		
	XFM01	XFM13	XFM25	TNIM-3	XFM13	XFM16
Length (μm)	10–30	10–30	10–20	20–100	10–30	0.5–2
Diameter (nm)	≤8	10–20	30–50	10–20	10–20	10–20
Aspect ratio	2500	1300	375	4000	1300	80

dimensions of 25 mm × 2 mm × 1 mm cutting from pressed plates were used. At least five samples were tested and the average results were reported.

Results and discussion

Dispersion of MWCNTs

Before melt mixing with OBC, the primary morphology of MWCNTs in Fig. S1 shows that all of MWCNTs exhibit bird nest structure. The SEM images of OBC nanocomposites containing MWCNTs with different aspect ratios based on the same length and the same diameter are shown in Fig. 1. At low loading of 1.0 vol%, homogeneous distribution of MWCNTs can be observed for MWCNTs with different aspect ratios based on the same length and the same diameter, and only very few small agglomerates appear in SL-2500-1.0, possibly due to that MWCNTs with high aspect ratios and small diameters behave high flexibility and are hard to untangle even under the action of shear force. At high loading of 4.5 vol%, for MWCNTs with high aspect ratio, small agglomerates and large agglomerates as the yellow circles marked appear in SL-2500-4.5 and SD-4000-4.5, respectively (Fig. 1b and h). With the aspect ratio reducing, homogeneous distribution of MWCNTs are presented in SL/SD −1300-4.5 and SL-375-4.5, and small agglomerates appear in SD-80-4.5. Moreover, MWCNTs in SL-375-4.5 and SD-80-4.5 seem to detach from the OBC matrix as marked by the red circles in Fig. 1d and j, probably owing to that rigid MWCNTs with low aspect ratios show weaker interactions with polymer matrix compared to MWCNTs with high aspect ratios [26]. The above-mentioned effect of difference in diameters of MWCNTs on the dispersion is consistent with the results of Ayatollahi et al. [26].

TEM observation was carried out to further reveal the dispersion of MWCNTs. Figures 2 and 3 shows TEM images of OBC nanocomposites containing MWCNTs with different aspect ratios based on the same length and the same diameter. For MWCNTs with high aspect ratios, the agglomerates of MWCNTs as marked by the yellow circles are observed for SL-2500-2 and SD-4000-2 as shown in Fig. 2a and d. For SL-2500-2, self-curled MWCNTs as shown in Fig. 3a are dispersed homogeneously in the OBC accompanied with some small agglomerates. The curled MWCNTs can provide contact points between small agglomerates of MWCNTs. For SD-4000-2, MWCNTs are dispersed as randomly bent fibers, and entangle with each other to form large bundles in Fig. 3d. The

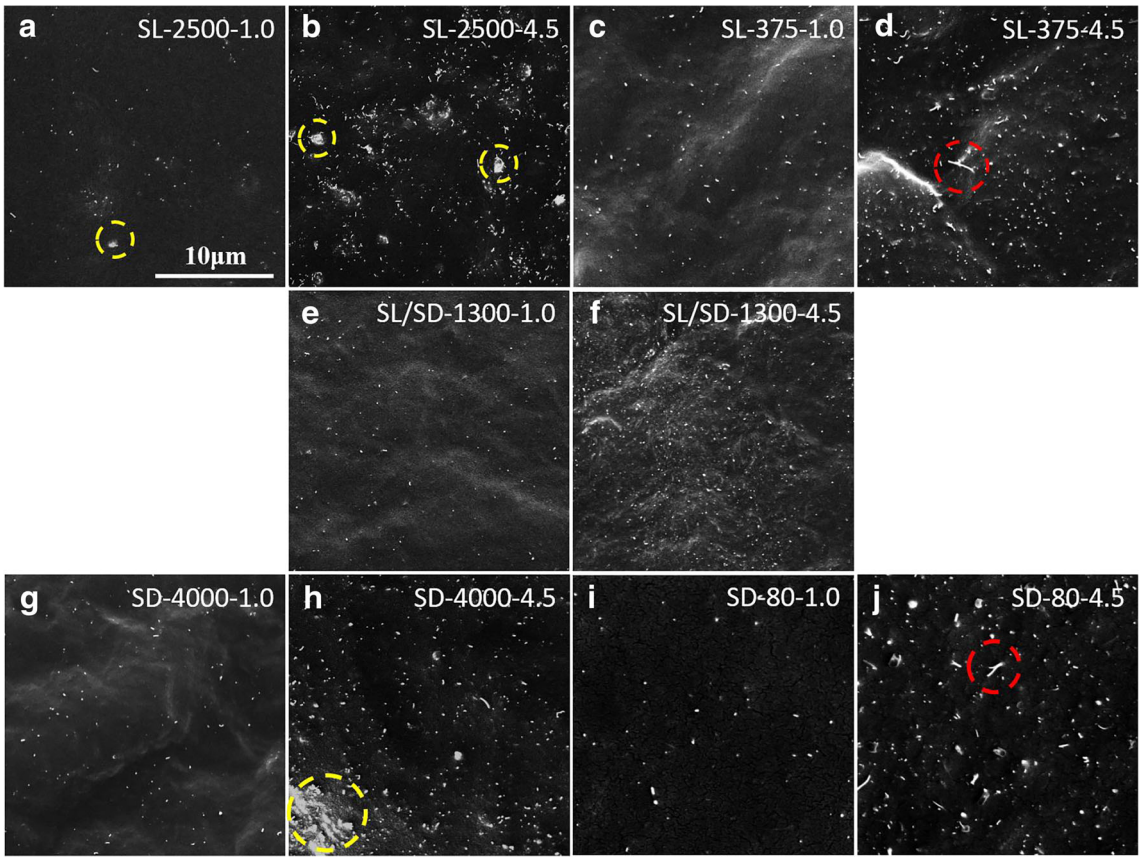

Fig. 1 SEM images of (a) SL-2500-1.0, (b) SL-2500-4.5, (c) SL-375-1.0, (d) SL-375-4.5, (e) SL-1300-1.0, (f) SL/SD-1300-4.5, (g) SD-4000-1.0, (h) SD-4000-4.5, (i) SD-80-1.0, (j) SD-80-4.5

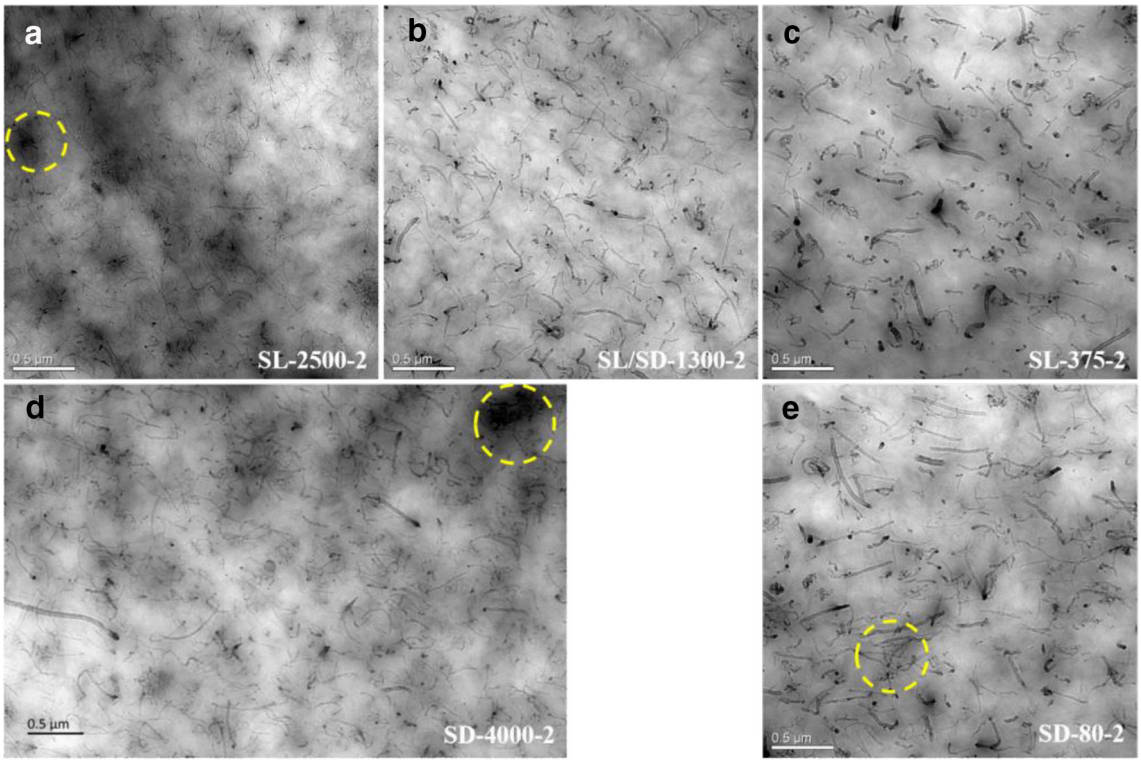

Fig. 2 TEM images of (a) SL-2500-2, (b) SL/SD-1300-2, (c) SL-375-2, (d) SD-4000-2, (e) SD-80-2. The yellow circles indicate the MWCNTs agglomerates

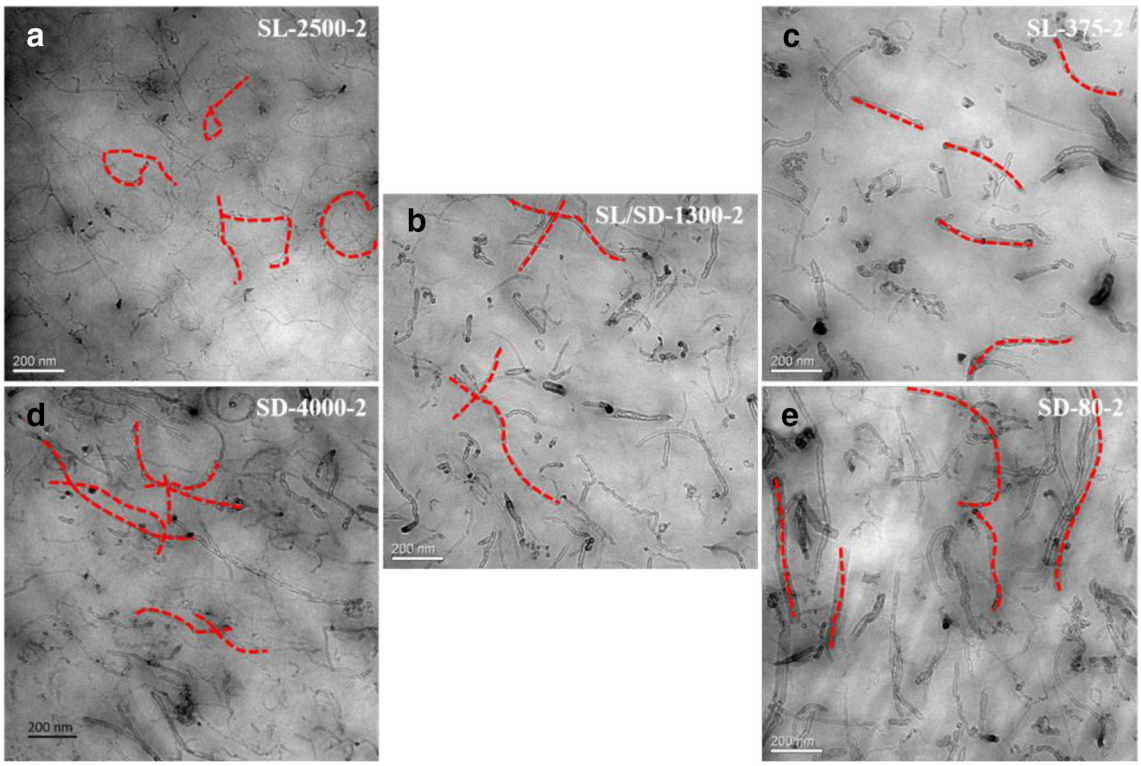

Fig. 3 Amplified TEM images of (a) SL-2500-2, (b) SL/SD-1300-2, (c) SL-375-2, (d) SD-4000-2, (e) SD-80-2. The red lines represent the MWCNTs morphology. The scale is 200 nm. The morphology and distribution of MWCNTs are marked to guide the eye by red lines

locally bridged network can be formed by closely inter-entangled MWCNTs as shown in Fig. 3d. With the aspect ratio reducing, MWCNTs are dispersed mainly as independent individuals, and the bridge of MWCNTs locally can form the loose interconnecting structure for SL/SD-1300-2 as shown in Fig. 2b and 3b. The observed homogeneous distribution of SL/SD-1300 in OBC is well consistent with our previous results [34]. For SL-375-2 and SD-80-2, MWCNTs tend to be straight and aligned as stiff fibers as marked by the dashed lines as shown in Fig. 3c and e, indicating a dilute or semi-dilute state with far lower volume fraction than that of MWCNTs with high aspect ratios. The bridge between MWCNTs is hard to be observed for SL-375-2, and the connection of MWCNTs also cannot be formed for SD-80-2 though the MWCNTs agglomerates occur locally in Fig. 2c and e. These results are well consistent with the SEM results, demonstrating that the agglomerates of MWCNTs can occur for not only MWCNTs with high aspect ratios, but also those with low aspect ratios, depending on the complex interactions between nanotube-nanotube and the nanotube-polymer.

Figure 4 describes the dispersion of MWCNTs with different aspect ratios schematically. The dispersion of MWCNTs in polymer composites is influenced by the nanotube-nanotube and the nanotube-polymer interactions and nanotubes themselves. MWCNTs with high aspect ratios behave strong nanotube-polymer interactions maybe due to larger interface between single MWCNT and polymer matrix, beneficial for the dispersion of MWCNTs and the construction of networks in polymer matrix. Moreover, the dispersion also is affected by the nanotube-nanotube interactions. MWCNTs with high aspect ratio and smaller diameter have strong intra-entanglement due to the high flexibility of MWCNTs, and are dispersed as self-entangled flocs in SL-2500 as shown in Fig. 4a. Homogeneously dispersed MWCNTs as independent individuals can form the loose interconnecting structure in SL/SD-1300 as shown in Fig. 4b. The low aspect ratios of MWCNTs makes the bridging of MWCNTs hard for SL-375 in Fig. 4c. MWCNTs with high aspect ratio and larger diameter have inter-entanglement among themselves, and large agglomerates are formed locally in SD-4000 in Fig. 4d. The weak nanotube-polymer interactions possibly resulting from reduced interface between single MWCNT and polymer matrix, leads to the local MWCNTs agglomerates occurring for MWCNTs with low aspect ratio in SD-80 in Fig. 4e.

Rheological behavior

Rheological measurements can be utilized to analyze the filler-polymer and filler-filler interactions and the dispersion of MWCNTs in polymer/MWCNTs composites [34, 38, 39]. To reveal the network formation and dispersion of MWCNTs in OBC nanocomposites, dynamic rheological behavior were measured at 150 °C and the results are shown in Fig. 5.

Figure 5a shows the frequency dependence of the storage modulus (G') for OBC nanocomposites containing MWCNTs with different aspect ratios based on the same length. At low frequencies, the storage modulus of OBC nanocomposites are higher than pure OBC obviously. The slopes derived in the terminal region of lgG'-lgω curve of pure OBC, SL-2500-2, SL-1300-2 and SL-375-2 are 0.943, 0.427, 0.484 and 0.885. The decrease of the slopes indicates that the long-range motions of the polymer chains are restrained in the presence of MWCNTs [40, 41]. The slopes decrease as the aspect ratio increasing at low loading of 2.0 vol%, which demonstrates

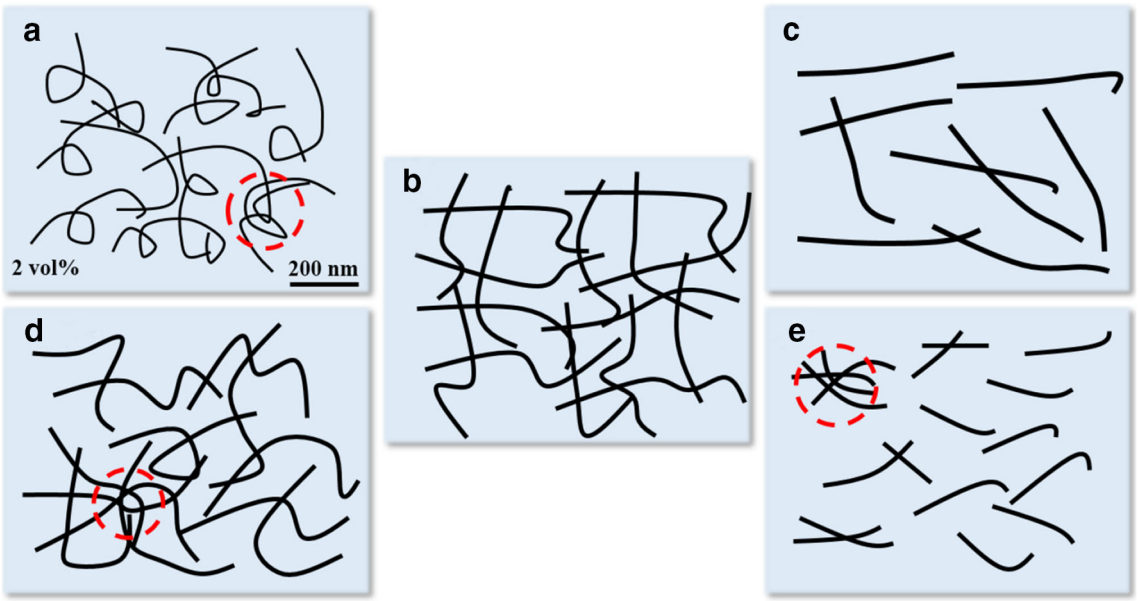

Fig. 4 Schematics of distribution of MWCNTs at the content of 2 vol% in (a) SL-2500, (b) SL/SD-1300, (c) SL-375, (d) SD-4000 and (e) SD-80. The solid lines and curves represent MWCNTs; the light blue background represent the OBC matrix; the red circles represent the agglomerates

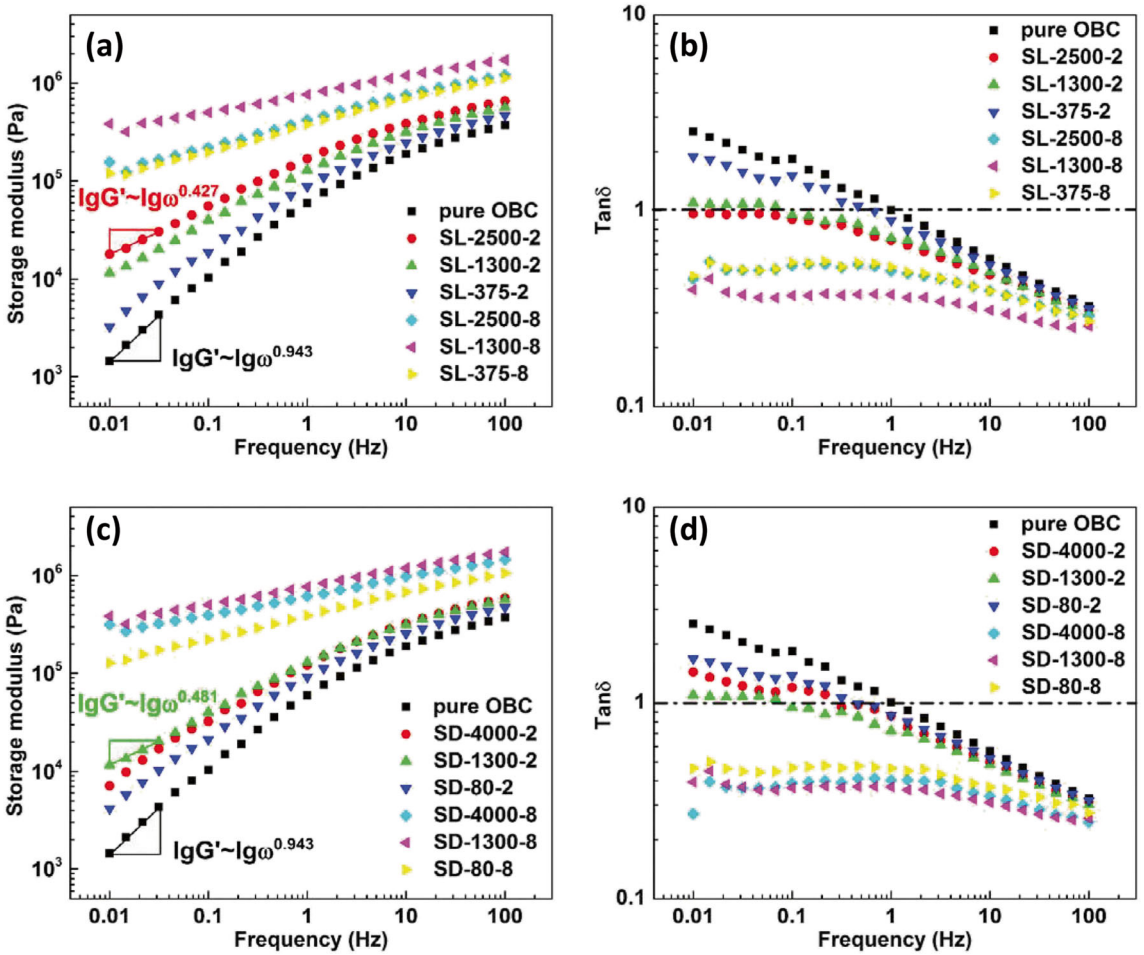

Fig. 5 (a) The storage modulus and (b) the loss tangent as a function of frequency for OBC nanocomposites containing MWCNTs with different aspect ratios based on the same length at different contents. (c) The storage modulus and (d) the loss tangent as a function of frequency for OBC nanocomposites containing MWCNTs with different aspect ratios based on the same diameter at different contents

that the network of MWCNTs with high aspect ratio in OBC nanocomposites is better developed than that of MWCNTs with low aspect ratio, then a more effective restraint of large-scale polymer relaxations appears in OBC nanocomposites containing MWCNTs with high aspect ratio.

Figure 5b gives the relationship between the loss tangent (tanδ) for OBC nanocomposites containing MWCNTs with the same length at different contents with oscillatory frequency. Tanδ is used to characterize the viscoelasticity of a material, and lower tanδ means that the composite is exhibiting more solid-like behavior. It is observed that the addition of MWCNTs induces the decrease of tanδ in Fig. 5b, indicating that the nanocomposites transform from liquid-like to solid-like state [42]. Tanδ decreases as the aspect ratio increases at low loading of 2.0 vol%, even the tanδ of SL-2500-2 is lower than 1, consistent with the results of storage modulus, revealing a more densely packed network in the composites containing MWCNTs with high aspect ratio. The MWCNTs with high aspect ratio are dispersed as randomly bent fibers and self-entangled flocs, presenting larger hydrodynamic radius than that of the MWCNTs with low aspect ratio due to their very high aspect ratio, which is responsible for higher effective volume fraction and stronger rheological responses of their composites.

With the MWCNTs loading increased to 8.0 vol%, the slopes derived in the terminal region of lgG'-lgω curve decreases and the G' is almost independent of frequency at low frequencies, which is indicative of a transition of liquid-like to solid-like behavior [43, 44]. This nonterminal low frequency behavior is regarded to be resulted from the formation of MWCNT network as the loading of MWCNTs increases, which restrains the long-range motion of the polymer chains. Moreover, it is noted that G' of SL-1300-8 is higher than that of SL-2500-8 though the latter has higher aspect ratio, indicating that the formation of agglomerates induced by self intra-entangled MWCNTs as shown by SEM and TEM observations, influences the network constructing at high MWCNTs loading.

Rheological behavior of OBC nanocomposites containing MWCNTs with different aspect ratios based on the same diameter are shown in Fig. 5c and d. At low and high loading MWCNTs, G' of SD-4000 is lower than that of SD-1300, also indicating that the formation of large agglomerates in SD-4000 as shown in SEM and TEM influences the development of network seriously. On the other hand, the MWCNTs in SD-4000 may be likely to break or shorten during mixing due to their large length, also causing the storage modulus of SD-4000 to be lower than those of SD-1300. From Fig. 5d, SD-1300 behaves more solid-like than SD-4000 and SD-80 at low and high loading of MWCNTs, due to the network in SD-1300 is well developed. These results are well consistent with the results of storage modulus.

Electrical properties

Figure 6a and c depict the conductivity (σ) as a function of the content of MWCNTs in OBC nanocomposites containing MWCNTs with different aspect ratios based on the same length and the same diameter. The conductivities of the composites increase with increased content of MWCNTs. The sudden change of conductivities appeared in the nanocomposite is generally described by a scaling law according to classical percolation theory [45–47] shown in Eq. (1),

$$\sigma = \sigma_0(\Phi - \Phi_c)^t \quad (1)$$

where σ_0 is a scaling factor, σ is the electrical conductivity of nanocomposites, t is the critical exponent revealing the dimensionality of the conductive networks, Φ is the volume content of MWCNTs, and Φ_c is the threshold of the electrical conductivity percolation. In order to get an estimate for Φ_c and the critical exponent t; the electrical conductivity data for $\Phi > \Phi_c$ were fitted according to Eq. (1).

The electrical conductivity percolation threshold, Φ_c, of conductive nanocomposites can be determined through fitting of the classical percolation theory to the experimentally obtained conductivity [48–50], as shown in Fig. 6b and d. SL-

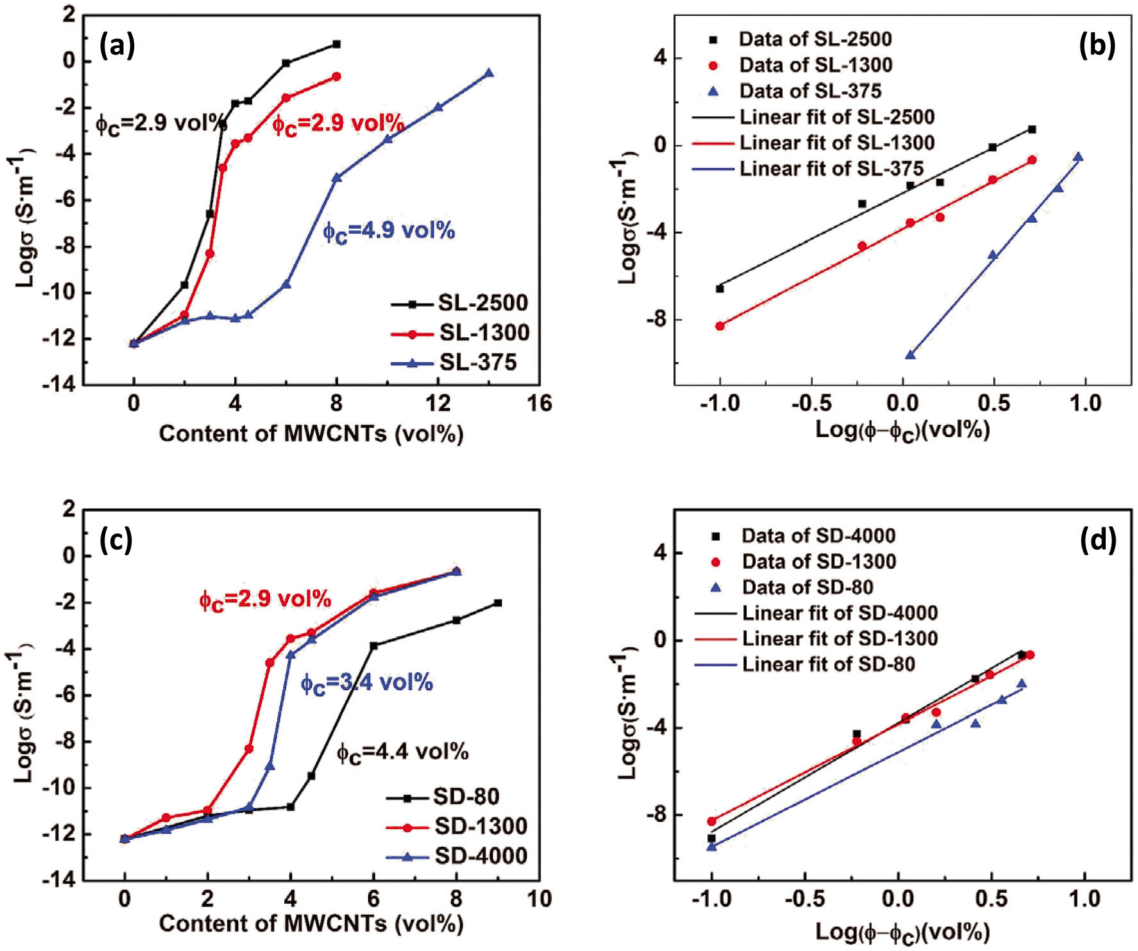

Fig. 6 (a) Log σ as a function of the content of MWCNTs and (b) a log-log plot of conductivity versus Φ-Φ_c and the fitting of the experimental results with the percolation law of OBC nanocomposites containing MWCNTs with different aspect ratios based on same length. (c) Log σ as a function of the content of MWCNTs and (d) a log-log plot of conductivity versus Φ-Φ_c and the fitting of the experimental results with the percolation law of OBC nanocomposites containing MWCNTs with different aspect ratios based on the same diameter

2500 and SL-1300 have the same percolation thresholds of 2.9 vol% which is relatively low, and the electrical conductivity of SL-2500 is higher than that of SL-1300 at the same content in Fig. 6a and b. Generally, the percolation threshold decreases with the aspect ratio of MWCNTs increases [47] and the results are consistent with those of Menzer et al. [32]. In Fig. 6c and d, the percolation threshold of SD-4000 is even higher than that of SD-1300. This contradiction implies that the formation of agglomerates, especially large agglomerates in SD-4000 influence the perfection of network, weakening the constructing of electrical network. It is obviously that the electrical conductivity of SL-4000 is actually lower than that of SL-1300 at the low content of MWCNTs. SL-375 and SD-80 present high percolation threshold, due to the MWCNTs with low aspect ratios, which tend to be straight and aligned as stiff fibers, are hard to form network locally and present poor conductivity for the composites. SL-375 has high percolation threshold than SD-80, due to even the locally connecting MWCNTs cannot be observed for SL-375 as SEM and TEM results shown in Figs. 1 and 2.

Tensile properties

The uniaxial stress-strain curves for all OBC/MWCNTs composites can characterize several of the tensile properties of typical thermoplastic elastomers, such as the diffused yielding point, strain-hardening at the late stage and large strain at break as shown in Fig. S2. The pure OBC shows lower stress at a certain stretching. With the addition of MWCNTs and the increased content of MWCNTs, stress at a certain stretching increases. The average values of the important tensile parameters are plotted versus the content of MWCNTs in the OBC nanocomposites containing MWCNTs with different ratios based on the same length and the same diameter in Fig.7. From Fig.7d and e, the improvement for Young's modulus and stress at 300% increases with the aspect ratios of MWCNTs increasing, indicating that MWCNTs with higher aspect ratio are beneficial for enhancing the modulus and strength of OBC nanocomposites due to the stronger nanotube-polymer interactions. The reinforcement role of MWCNTs depends on the load transfer from the matrix to MWCNTs and the interfacial strength. Stronger interface interaction leads to a better load transfer, which causes improved tensile properties. It is noted that though the agglomerates consisting of inter-entangled MWCNTs exist in SD-4000, and this inter-entanglement of MWCNTs has less effect on the nanotube-polymer interactions maybe due to the MWCNTs still can be wetted by polymer matrix, then showing less negative effect on the enhancing for the modulus and strength of the nanocomposites. In Fig.7a and b, Young's modulus and stress at 300% stretching for SL-1300 are higher than those of SL-2500, though the latter has higher aspect ratio. This is possibly due to the intra-entanglement among curled MWCNTs reduce the effective aspect ratio, showing

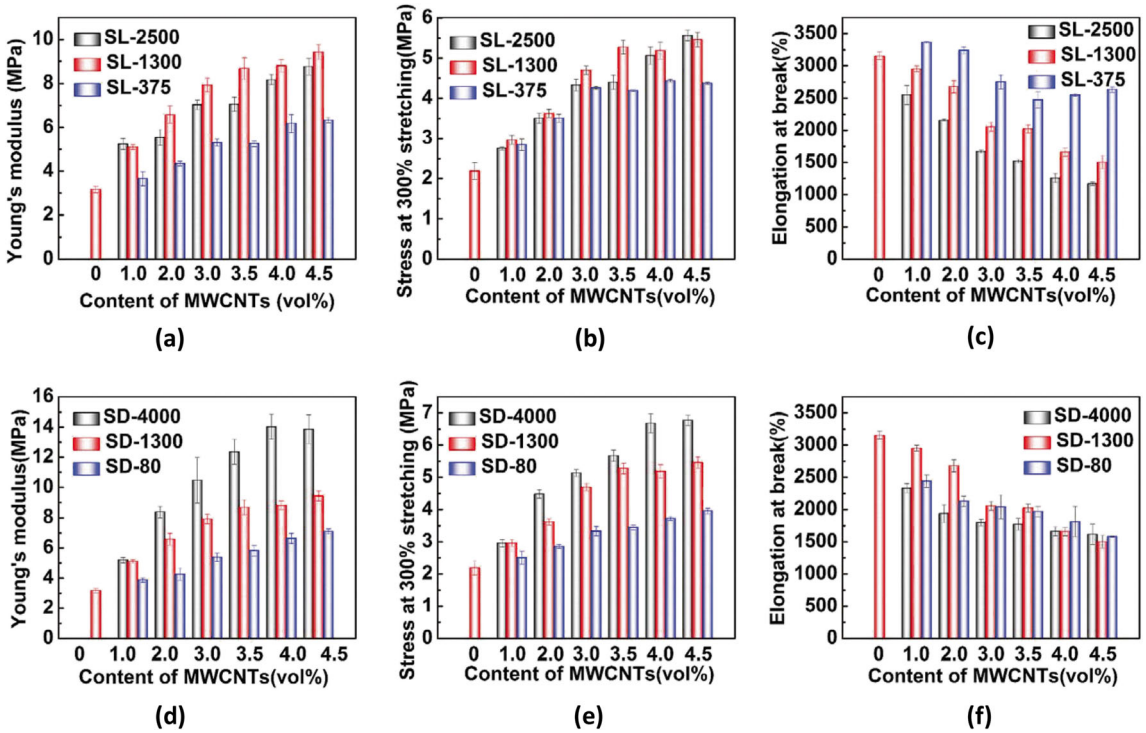

Fig. 7 (a) Young's modulus, (b) stress at 300% stretching and (c) elongation at break of OBC nanocomposites containing MWCNTs with different aspect ratios based on the same length. (d) Young's modulus, (e) stress at 300% stretching and (f) elongation at break of OBC nanocomposites containing MWCNTs with different aspect ratios base on the same diameter

discounted enhancing properties of nanocomposites. From Fig. 7c, the elongation at break decreases with the aspect ratios of MWCNTs increasing, demonstrating that the agglomerates or the bridged network of MWCNTs can cause concentrated stress and mechanical damage. It is also can be observed form Fig. 7f, the agglomerates of MWCNTs induces the elongation at break to decline rapidly for SD-4000 and SD-80.

Conclusions

MWCNTs with different aspect ratios were dispersed in OBC to prepare elastomeric composites through melt mixing. The effect of aspect ratios on the filler dispersion and properties of nanocomposites were investigated. The MWCNTs with high aspect ratio are beneficial for the dispersion of MWCNTs in polymer matrix. However, the MWCNTs with high aspect ratio and smaller diameter have strong intra-entanglement in themselves, and are dispersed as self-entangled agglomerates. The MWCNTs with high aspect ratio and larger diameter have inter-entanglement among themselves, and large agglomerates are formed locally. Rheological and electrical properties show that the MWCNTs with high aspect ratios tend to form network structure, but the formation of agglomerates weakens the constructing of rheological and electrical networks. MWCNTs with low aspect ratios tend to straighten and align as stiff fibers, and are hard to form network locally, presenting poor conductivity of composites. Furthermore, MWCNTs with high aspect ratio are beneficial for enhancing the modulus and strength of the OBC nanocomposites, but the intra-entanglement of MWCNTs shows discounted enhancing properties. This paper provides the guideline for the preparation of nanocomposites containing the MWCNTs with different sizes, paving the way to the diversified conductive elastomeric composites.

Acknowledgements This work was supported by the National Natural Science Foundation of China (NNSFC grants 51422305 and 51721091).

References

1. Iijima S (1991). Nature 354:56–58
2. Hou PX, Liu C, Cheng HM (2008). Carbon 46:2003–2025
3. Salvetat JP, Bonard JM, Thomson NH, Kulik AJ, Forro L, Benoit W, Zuppiroli L (1999). Appl Phys A-Mater Sci Process 69:255–260
4. Qian D, Wagner GJ, Liu WK, Yu MF, Ruoff RS (2002). Appl Mech Rev 55:495–533
5. Kaneto K, Tsuruta M, Sakai G, Cho W-Y, Ando Y (1999). Synth Met 103:2543–2546
6. Pop E, Mann D, Wang Q, Goodson K, Dai H (2006). Nano Lett 6: 96–100
7. Sang Z, Ke K, Manas-Zloczower I (2018). ACS Appl Mater Interfaces 10:36483–36492
8. Kumar S, Li B, Caceres S, Maguire R-G, Zhong W-H (2009). Nanotechnology 20:465708
9. Andrews R, Weisenberger M-C (2004). Curr Opin Solid State Mater Sci 8:31–37
10. Ounaies Z (2003). Compos Sci Technol 63:1637–1646
11. Dang ZM, Shehzad K, Zha JW, Mujahid A, Hussain T, Nie J, Shi CY (2011). Compos Sci Technol 72:28–35
12. Inukai S, Niihara K, Noguchi T, Ueki H, Magario A, Yamada E, Inagaki S, Endo M (2011). Ind Eng Chem Res 50:8016–8022
13. Liu Y, Li J, Pan Z (2011). J Polym Res 18:2055–2060
14. Garg P, Singh BP, Kumar G, Gupta T, Pandey I, Seth RK, Tandon RP, Mathur RB (2010). J Polym Res 18:1397–1407
15. Yang X, Zhan Y, Yang J, Zhong J, Zhao R, Liu X (2011). J Polym Res 19:9806
16. Ke K, Pötschke P, Wiegand N, Krause B, Voit B (2016). ACS Appl Mater Interfaces 8:14190–14199
17. Huang J, Mao C, Zhu Y, Jiang W, Yang X (2014). Carbon 73: 267–274
18. Cui W, Du F, Zhao J, Zhang W, Yang Y, Xie X, Mai YW (2011). Carbon 49:495–500
19. Liu H, Gao J, Huang W, Dai K, Zheng G, Liu C, Shen C, Yan X, Guo J, Guo Z (2016). Nanoscale 8:12977–12989
20. Chen Z, Qin Y, Weng D, Xiao Q, Peng Y, Wang X, Li H, Wei F, Lu Y (2009). Adv Funct Mater 19:3420–3426
21. Yin H, Dittrich B, Farooq M, Kerling S, Wartig K-A, Hofmann D, Huth C, Okolieocha C, Altstädt V, Schönhals A, Schartel B (2015). J Polym Res 22:140
22. Xu Y, Xu W, Bao J (2014). J Polym Res 21:543
23. Chi CH, Hsu YC, Tseng LC, Suen SY, Wu JY, Lee RH (2013). J Polym Res 20:269
24. Krause B, Barbier C, Kunz K, Pötschke P (2018). Polymer 159:75–85
25. Wu D, Wu L, Zhou W, Sun Y, Zhang M (2010). J Polym Scie Pt B-Polym Phys 48:479–489
26. Ayatollahi MR, Shadlou S, Shokrieh MM, Chitsazzadeh M (2011). Polym Test 30:548–556
27. Krause B, Mende M, Pötschke P, Petzold G (2010). Carbon 48: 2746–2754
28. Krause B, Petzold G, Pegel S, Pötschke P (2009). Carbon 47: 602–612
29. Guo J, Liu Y, Prada-Silvy R, Tan Y, Azad S, Krause B, Pötschke P, Grady BP (2014). J Polym Sci B Polym Phys 52:73–83
30. Castillo FY, Socher R, Krause B, Headrick R, Grady BP, Prada-Silvy R, Pötschke P (2011). Polymer 52:3835–3845
31. Krause B, Villmow T, Boldt R, Mende M, Petzold G, Pötschke P (2011). Compos Sci Technol 71:1145–1153
32. Menzer K, Krause B, Boldt R, Kretzschmar B, Weidisch R, Pötschke P (2011). Compos Sci Technol 71:1936–1943
33. Zhai Y, Zhang R, Yang W, Yang M (2017). Polymer 114:44–53
34. Li T, Pu JH, Ma LF, Bao RY, Qi GQ, Yang W, Xie BH, Yang MB (2015). Polym Chem 6:7160–7170
35. Zha XJ, Pu JH, Ma LF, Li T, Bao RY, Bai L, Liu ZY, Yang MB, Yang W (2018). Compos Pt A-Appl Sci Manuf 105:118–125
36. Zha XJ, Li T, Bao RY, Bai L, Liu ZY, Yang W, Yang MB (2017). Compos Sci Technol 139:17–25
37. Krause B, Carval J, Pötschke P (2017) AIP Conf Proc 1914: 030007–030001–030007-030005
38. Zhang QH, Fang F, Zhao X, Li YZ, Zhu MF, Chen DJ (2008). J Phys Chem B 112:12606–12611
39. Huang CL, Wang C (2011). Carbon 49:2334–2344
40. Seo MK, Park SJ (2004). Chem Phys Lett 395:44–48
41. Kim JA, Seong DG, Kang TJ, Youn JR (2006). Carbon 44: 1898–1905
42. Song YS (2006). Rheol Acta 46:231–238
43. Pötschke P, Fornes TD, Paul DR (2002). Polymer 43:3247–3255
44. Pötschke P, Abdel-Goad M, Alig I, Dudkin S, Lellinger D (2004). Polymer 45:8863–8870

45. Koerner H, Liu WD, Alexander M, Mirau P, Dowty H, Vaia RA (2005). Polymer 46:4405–4420
46. Tan Y, Fang L, Xiao J, Song Y, Zheng Q (2013). Polym Chem 4: 2939–2944
47. Bauhofer WG, Kovacs JZ (2009). Compos Sci Technol 69: 1486–1498
48. Zhang J, Mine M, Zhu D, Matsuo M (2009). Carbon 47:1311–1320
49. Wang Q, Dai J, Li W, Wei Z, Jiang J (2008). Compos Sci Technol 68:1644–1648
50. Spitalsky Z, Tasis D, Papagelis K, Galiotis C (2010). Prog Polym Sci 35:357–401